JOURNAL OF GEOPHYSICAL RESEARCH, VOL. 108, NO. D23, 4741, doi:10.1029/2003JD003392, 2003

Three-dimensional radiative transfer in tropical deep convective clouds

F. Di Giuseppe
Environmental Systems Science Centre, University of Reading, Reading, UK

A. M. Tompkins
European Centre for Medium-Range Weather Forecasts, Reading, UK

Received 9 January 2003; revised 27 June 2003; accepted 14 July 2003; published 12 December 2003.

[1] This study focuses on the interaction between short-wave radiation and a field of tropical deep convective clouds generated using a cloud-resolving model to assess the significance of three-dimensional radiative transport. Comparisons with an independent pixel approximation approach and a plane-parallel radiative scheme are used to assess the importance of the subgrid-scale variability and organization of the clouds for their radiative properties. The horizontal transport of radiation is responsible for a significant energy redistribution inside the cloudy and clear regions. Local heating rates in both the cloudy and clear-sky regions can differ by 1 K d^{-1} or more, with mean heating rates altered by 20% and 15%, respectively. These figures are larger than previously reported for convective scenes, most probably because of the lower cloud fraction of the scene used here. This energy imbalance is mainly controlled by two opposing effects: side illumination and shadowing, whose relative importance is driven by the spatial arrangement of cloud elements in the domain, the Sun position and the aspect ratio of clouds. These effects partially cancel, giving lower mean biases. Nevertheless, comparison between independent pixel approximation and plane-parallel biases shows that for deep convective cloud, geometry-related effects can have a larger influence on radiative transfer calculation than internal optical inhomogeneities. *INDEX TERMS:* 3359 Meteorology and Atmospheric Dynamics: Radiative processes; 3314 Meteorology and Atmospheric Dynamics: Convective processes; 3374 Meteorology and Atmospheric Dynamics: Tropical meteorology; *KEYWORDS:* 3-D radiative transfer, convective clouds

Citation: Di Giuseppe, F., and A. M. Tompkins, Three-dimensional radiative transfer in tropical deep convective clouds, *J. Geophys. Res.*, *108*(D23), 4741, doi:10.1029/2003JD003392, 2003.

1. Introduction

[2] The calculation of radiative fluxes in general circulation models (GCMs) is complicated by the presence of clouds, which have complex radiative properties. Since clouds occur on smaller scales than present global model grid sizes, and therefore must themselves be parameterized, even basic quantities such as the mean liquid water content or cloud cover are uncertain.

[3] Even if cloud properties for a GCM grid point were perfectly known, it would be prohibitively computationally expensive to perform an exact full three-dimensional line-by-line radiative transfer calculation, and therefore a number of approximations are made. In the plane-parallel (PP) approximation neither the optical variability nor the horizontal subgrid-scale location of the clouds are taken into account. Vertical radiative fluxes are generally calculated separately for the clear-sky and cloudy parts of the GCM grid-box. An improvement on the plane-parallel approach is offered by the independent pixel approximation (IPA), which attempts to account for the subgrid-scale optical variability by taking the average of many PP column calculations for a much higher horizontal resolution grid. In this way, radiative biases in cloud optical properties such as reflection, which are nonlinear functions of cloud water content, can be reduced [*Cahalan et al.*, 1994a, 1994b]. The IPA was found to improve radiative flux calculations in stratocumulus boundary layer clouds [*Cahalan et al.*, 1994a; *Barker et al.*, 1998; *Marshak et al.*, 1998; *Fu et al.*, 2000]. The difference between the standard PP calculation and the IPA result is also termed the "PP bias."

[4] Despite its obvious advantage over the PP calculation, the IPA does not consider the horizontal geometrical cloud arrangement and does not allow for the horizontal transport of photons. The cloud fraction in stratocumulus regimes for which IPA was mostly tested equals or approaches unity, and therefore horizontal radiative transport could be expected to play a relatively minor role. If a more complex cloud regime is considered, where clouds are separated by clear regions, then other effects have to be considered: cloud shadowing, cloud-cloud interaction and the vertical arrangement are examples.

0148-0227/03/2003JD003392$09.00

[5] Several studies on complex broken cloud arrangements have been conducted, some using idealized techniques to create the cloud field [*McKee and Cox*, 1974; *Aida*, 1977; *Welch and Wielicki*, 1985; *Kite*, 1987; *Welch and Wielicki*, 1989; *Marshak et al.*, 1998], while other investigations used fields generated from satellite imagery [*Coakley and Davies*, 1986; *O'Hirok and Gautier*, 1998a, 1998b; *Fu et al.*, 2000; *Vogelmann et al.*, 2001]. The implication of these studies was that the radiative properties of the atmosphere can undergo a substantial change when the aspect ratio of the cloud elements approaches unity. Especially in the short-wave, where scattering is important, the horizontal transport of photons can become significant as the cloud dimension approaches the mean photon path length. This can be assessed by comparing suitable IPA and three-dimensional (3-D) calculations and is termed the "IPA bias." (Often relative biases are used, defined as $100 \times$ (3-D $-$ IPA)/IPA for the IPA bias [*Cahalan et al.*, 1994b], and similarly for the PP bias.) For instance, *Titov* [1998] and *Marshak et al.* [1998] proved how neglecting horizontal transport can produce substantial biases in the interpretation of data obtained by aircraft measurements, and *Davis et al.* [1997] showed similar shortcomings in cloud properties retrieved from satellite.

[6] Considering these studies some basic questions arise. The first concerns the validity of the two-stream approximation, especially as the GCM resolution approaches the mesoscale. Another issue is the scale at which the divergence and organization of horizontal photon transport becomes nonnegligible and the relevance of 3-D effects if models include a representation of subgrid-scale cloud variability.

[7] Any errors involved in the neglect of horizontal transfer are expected to be maximized in deep convective systems, particularly prevalent in the tropics and midlatitude summers. Whether present in the form of isolated or clustered thunderstorms or organized into larger-scale systems such as squall lines or tropical cyclones, these deep convective regimes are characterized by large horizontal variability both in terms of water vapor and cloud mass over large length scales in both the horizontal and vertical [*Liao and Rind*, 1997; *Brown and Zhang*, 1997]. It is not currently known what magnitude of error is involved when a two stream approximation is used to describe the radiative transfer through such a cloud field but it seems likely that these situations will be complex to represent.

[8] This paper therefore focuses on the interaction between short-wave radiation with a field of tropical deep convective events. Previously, satellite and radar observations have been used to reconstructive convective cloud scenes. Although capable of rendering reasonable representations of shallow systems [*Chambers et al.*, 1997], satellite data does not currently provide sufficient vertical resolution to provide a realistic 3-D description of a deep convective system. Both *O'Hirok and Gautier* [1998a] and *Vogelmann et al.* [2001] found it necessary to assume a constant extinction through all clouds, effectively neglecting in-cloud vertical heterogeneity. The cloud upper or lower boundaries were then fixed by the optical depth, and the cloud geometry is consequently sensitive to the assumed homogeneous extinction coefficient. Bearing these caveats in mind, *O'Hirok and Gautier* [1998a] reported a significant relative IPA albedo bias of 7% and a maximum absorptance enhancement of 15 W m^{-2}, and indicated that neglecting horizontal transport can produce unrealistic results when complex geometrical cloud arrangements are considered. *Vogelmann et al.* [2001] emphasized the large variation of heating rate that occurred over scales much smaller than current climate models resolve.

[9] Radar data does not have the drawback of poor vertical resolution, but current retrievals of liquid and ice mass directly from radar reflectivity suffer from considerable uncertainty of as much as 100% [*Brown and Swann*, 1997; *Mace et al.*, 1998; *Sassen et al.*, 2002], although taking other information into account can considerably reduce this error [*Sassen et al.*, 2002; *Wang and Sassen*, 2002; *Liou et al.*, 2002; *Benedetti et al.*, 2003]. Sometimes only a two-dimensional view is provided [*Zuidema and Evans*, 1998], and a concurrent assessment of the temperature and water vapor vertical structure is often lacking, which would require a separate data source such as a co-located radiosonde ascents. *Carlin et al.* [2002] examined the plane-parallel bias in two-dimensional high cloud with optical depths less than 5 and found biases of as much as 25%, but no assessment of the IPA bias was made.

[10] An alternative approach is adopted here of using a three-dimensional cloud-resolving model (CRM) simulation to provide a proxy for a deep convective cloud field. This method is also open to criticism since the achievable realism of such model simulations is still under considerable debate, and the simulated cloud dynamical and thermodynamical properties are sensitive to many uncertain parameterizations, most notably the microphysics of the ice-phase [*Emanuel*, 1994]. A number of investigations show that the quality of the representation of cloud microphysics in CRMs can be reasonable and is roughly comparable to the accuracy of the simpler radar retrieval algorithms based solely on reflectivity [*Phillips et al.*, 2001; *Benedetti and Stephens*, 2001; *Luo et al.*, 2003] and such models have already been used to provide proxy data sets for the development of retrieval techniques [*Ovtchinnikov and Kogan*, 2000; *Sassen et al.*, 2002]. In particular, the model used in this study has been applied with reasonable success to the simulation of ice clouds in a variety of situations [*Swann*, 1998; *Brown and Heymsfield*, 2001]. More generally, studies have demonstrated the ability of these models to reliably simulate a considerable variety of organized and unorganized convective situations [*Grabowski et al.*, 1998; *Donner et al.*, 1999; *Redelsperger et al.*, 2000; *Montmerle et al.*, 2000; *Diongue et al.*, 2002]. Overall, the view is taken the zero-order effect of 3-D radiative transfer can be reasonably assessed using such a simulated cloud field, even if the details, such as in-cloud condensate amount and cirrus anvil extent, may not be exact. Thus studies using model generated fields can usefully supplement those based on observational data.

[11] *Fu et al.* [2000] used a 2-D CRM model to conclude that the IPA bias was small over length scales comparable to the GCM grid. However, one drawback of 2-D models was pointed out by *Tompkins and Craig* [1998] and *Tompkins* [2000], namely that without the use of open lateral boundary conditions or excessive large-scale forcing, extensive domains of several thousand kilometers in extent are required to prevent the intermittency of the deep convection.

This could lead to an underestimation of 3-D radiative transfer effects. *Barker et al.* [1999] used a 3-D CRM to provide the cloud system field. However, the CRM used in this system used a parameterization of microphysical processes that produced high cloud fractions approaching 100%. This would minimize the consequence of horizontal photon transport and thus it is not surprising that the IPA bias was assessed to be limited in such cloud systems, although *Fu et al.* [2000] did highlight that local biases could be much more significant. *Barker et al.* [1998] also used a 3-D model, but one that again produced a very extensive cloud shield at midlevels.

[12] While the virtually overcast scenes used by *Barker et al.* [1999] may render a reasonable estimate of radiative biases for mesoscale convective systems, that may produce anvil shield extending hundreds or even thousands of kilometers, a lower cloud fraction is likely to be more representative of unorganized deep convective scenarios consisting of isolated thunderstorms [*Byers and Braham*, 1948; *Houze*, 1981; *Zhang*, 1993]. Studies of precipitation radar statistics, while not able to detect the full extent of cirrus anvil regions, do show that the vast majority of precipitating systems in the Western Pacific are organized on horizontal spatial scales inferior to 25 km [*Rickenbach and Rutledge*, 1998; *Johnson et al.*, 1999]. The present article therefore aims to re-examine the significance of horizontal radiative transport using a cloud field generated by a 3-D model that produces much lower cloud covers of around 20% that may be more representative of these unorganized deep convective situations. Additionally, the present model also uses a horizontal resolution finer than previously used to ensure subcloud structure is well resolved.

[13] The paper is arranged as follows: Section 2 gives a brief description of the radiation code and of the CRM simulation used to generate the cloud data field. Section 3 reports the diagnosis of the 3-D radiative transfer calculation using this deep convective cloud field. The following section 4 then proceeds to compare the 3-D results with those obtained using the IPA and a GCM type PP calculation, respectively. In section five the conclusions are drawn.

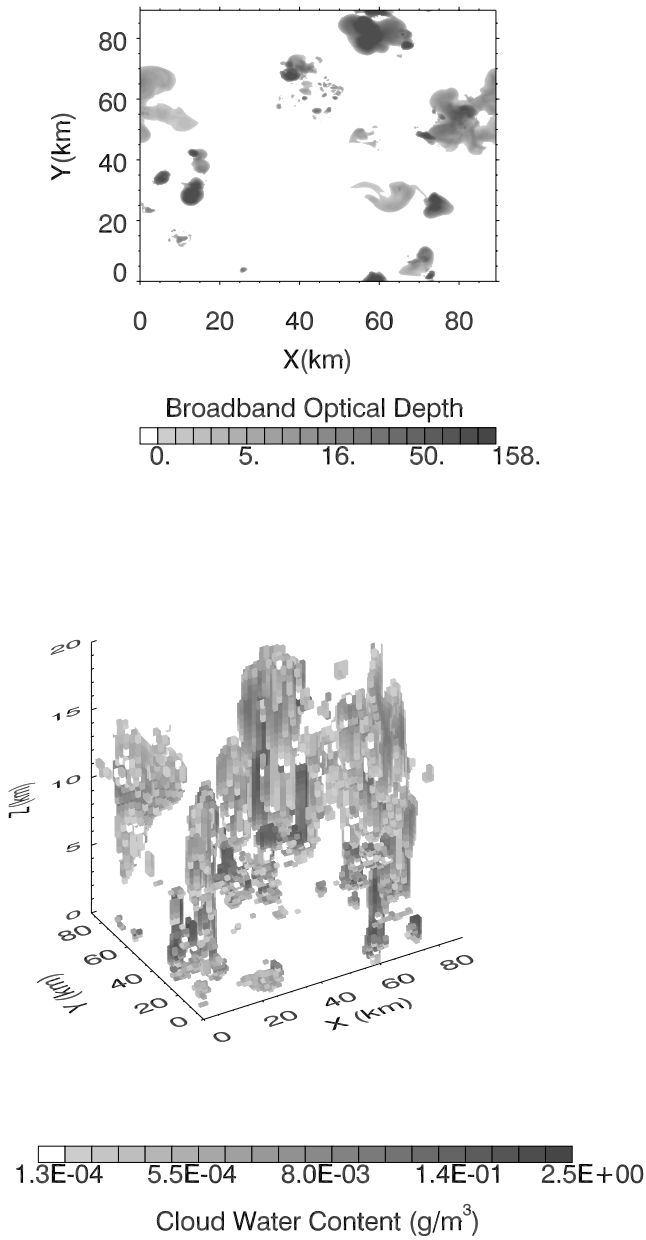

Figure 1. (top) Plane view of the SW optical thickness for the CRM experiment. (bottom) Three-dimensional rendition of the cloud liquid and ice content generated with the CRM. Read 1.3E-04 as 1.3×10^{-4}.

2. Model and Data Description

2.1. Data Description

[14] The cloud field in this study is taken from the 3-D CRM experiments of *Tompkins* [2001] for a situation of deep convection in quasi equilibrium with its forcing. Details of the dynamical framework of the model are given by *Shutts and Gray* [1994]. Cloud microphysical processes are parameterized according to *Brown and Swann* [1997], which includes prognostic equations for the mass mixing ratio of total water (liquid cloud plus vapor), snow, rain, graupel and cloud ice, as well as the cloud ice number concentration. Comparisons of simulations to observed cloud properties with this model have been encouraging [*Brown and Swann*, 1997; *Swann*, 1998; *Brown and Heymsfield*, 2001].

[15] The experiments used a relatively high horizontal resolution of 350 m over a square domain of $L(x) = 89.6$ km by $M(y) = 89.6$ km, with a vertical resolution stretching from 100 m in the boundary layer to 500 m from the midtroposphere to the domain lid at 21 km altitude. The lower boundary condition is a fixed temperature ocean of 300 K, and the horizontal boundary conditions are cyclic. The deep convection is forced by a constant cooling of 2 K d^{-1} throughout the troposphere, sufficient for the domain to always contain several coexisting active deep convective systems, in addition to cirrus remnants of previous systems and much boundary layer cloud. This is clear from Figure 1, which gives a three-dimensional rendition of the cloud liquid and ice content. The figure also shows the broadband optical thickness (τ_b) throughout the CRM domain and reveals that the maximum cloud cover is relatively small, at approximately 20%. The

broadband optical thickness is calculated as a weighted mean of the optical thickness in each of the six short wavelength (SW) spectral bands according to $\tau_b = \log[\Sigma S_i e^{-\tau_i}/\Sigma S_i]$, where S_i is the solar radiance in the ith SW band. The relatively low cloud fraction is a result of the zero mean wind shear applied in this idealized simulation, although such details as anvil extent are also sensitive to uncertain assumptions of the ice microphysics.

2.2. Radiative Calculation

[16] The radiative transfer calculation have been performed using SHDOM, which is described in detail by *Evans* [1998]. In contrast to Monte Carlo methods, SHDOM explicitly solves the radiative transfer equation over a regular grid. At each grid point the radiative source function is represented in spherical harmonics, which is converted to discrete ordinates and integrated to determine the radiances. Most radiative quantities can be consequently calculated from the spherical harmonic representation of the source function.

[17] Along each angular direction, the cloud liquid (or ice) water content is obtained by interpolation between grid points. This could lead to inaccuracy where strong gradients exist, for instance at cloud boundaries. This situation can be avoided by splitting such cells into a number of subgrid cells. Thus the accuracy of the model calculation is driven by the angular resolution and the spatial grid splitting threshold. This study adopts a medium angular resolution ($N_\mu = 8$, $N_\phi = 16$, where μ and ϕ represent the zenith and azimuth integration angles), since hemispherical integrated fluxes are mainly considered, while a sensitive cell splitting threshold that only allows a 10% variation in cloud properties between cells is used, to handle the highly variable source function that exists in such a cloud field. Only the cloud mass varies in the horizontal; water vapor and temperature are functions of height and thus the cell splitting algorithm does not operate in the clear-sky regions. The same base grid as the CRM is therefore adopted, with a horizontal resolution of 350 m.

[18] Although the achievable accuracy using a spherical harmonics approach is less than that of Monte Carlo methods, the advantage offered is the possibility of simultaneous calculation of multiple radiative diagnostics, such as fluxes integrated in any direction, directional radiances and heating rates. The main reason that spherical harmonic codes have not been previously used with the large domains necessary for studying deep convective systems is the prohibitive memory resources required (scaling with the product of the number of grid points and the angular resolution). In order to assess the numerical accuracy using this setup, initial sensitivity tests were performed using one quarter of the CRM domain (45.8×45.8 km^2). This included a very high resolution calculation using $N_\mu = 24$ and $N_\phi = 32$ and a cell splitting threshold of 1%. Comparisons with a run using the standard resolution revealed differences in the integrated upwelling and downwelling fluxes of 2%. The maximum difference in the heating rates calculated from the net flux divergence was 3%, which was also the assessment of the error in energy conservation. SHDOM has also been compared extensively with a number of other 3-D radiation codes, many based on Monte Carlo methods, and has been found to render comparable results for a variety of simple cloud arrangements [*Evans*, 1998].

[19] Mie theory is used for both water (w) and ice (i), and the single scattering albedo ($\overline{\omega_0}$) and the phase function (P) for the mixed phase are defined in term of the total extinction coefficient ($k = k_w + k_i$) as usual:

$$\overline{\omega_0} = (\overline{\omega_{0w}} k_w + \overline{\omega_{0i}} k_i) k^{-1} \tag{1}$$

$$P = \frac{\overline{\omega_{0w}} k_w P_w + \overline{\omega_{0i}} k_i P_i}{\overline{\omega_{0w}} k_w + \overline{\omega_{0i}} k_i} \tag{2}$$

The particle size distribution is modeled using a Gamma distribution with effective radius ranging between 0.5 and 25 μm (mode equal to 10 μm) for the water droplets and 10 and 50 μm (mode equal to 30 μm) for the ice crystals, being in both cases constrained by the constant particle concentration numbers of 50 and 30 cm^{-3}, respectively. This different treatment between ice and water avoids the unrealistic increase of the optical depth (τ) inside the towering clouds experienced when a constant effective radius approximation is considered. The maximum value for τ_b is 200, with a mean value of 70. An alternative approach for the ice phase would have been to directly use the ice number concentration prognosed by the CRM, but it was found that this lead to unreasonable values of the effective radius in some cases. The surface is assumed to be ocean as per the CRM simulation scenario and thus for simplicity the surface albedo is set to zero.

[20] A multispectral band calculation is used, according to the k-distribution model of *Fu and Liou* [1992]. Six bands cover the solar part of the spectrum (0.2–4 μm). Gaseous absorption for ozone, CO_2, CH_4, and N_2O is included as horizontally homogeneous. Layer mean water vapor and temperature values are obtained from the CRM, while above the CRM domain seven additional atmospheric levels are placed between 20 km to 100 km which are interpolated using tropical standard profiles [*McClatchey et al.*, 1972]. Rayleigh scattering is also included.

[21] Two experiments have been performed for the solar zenith angles of 0 (Sun overhead) and 60 degrees, which in the interest of brevity in the following discussion are referred to as cases "SZA0" and "SZA60," respectively. On the same CRM convective cloud field two different 1-D radiative calculations have been performed; the independent pixel approximation (IPA) and the plane-parallel (PP) approximation, similar to that implemented in most GCMs.

[22] The IPA calculation is performed by modifying the SHDOM algorithm to impose local periodic boundary conditions in each separate column of the CRM domain. With this procedure the horizontal transport of radiation between neighboring cells is inhibited, while the assumptions for the radiative calculations are left identical to those used in the full 3-D case. As outlined in the introduction, such an IPA calculation can still appreciate horizontal variability in cloud condensate, but will be unaffected by the geometrical arrangement of the cloud, because of the independence of each column.

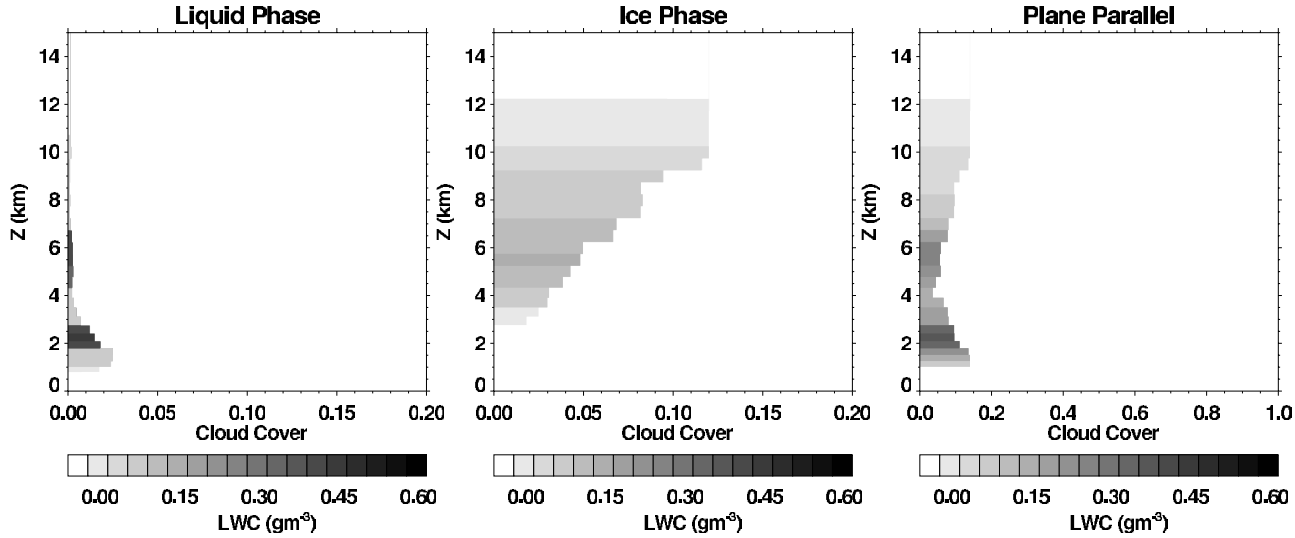

Figure 2. Reduction of the CRM scene for the plane-parallel (PP) calculation. The liquid phase and ice phase are treated separately and then added together according to their cloud covers.

[23] The PP calculation is performed by first horizontally averaging the cloud condensate mass at each height and rearranging the clouds according to the maximum-random overlap rule commonly applied in GCMs [e.g., *Stubenrauch et al.*, 1997]. Examining the cloud overlap at each height, the atmosphere is then divided up into the number of columns required to capture the vertical cloud structure. The radiative transfer is then performed separately for each of these columns as for the IPA mode. Since this experiment has 31 vertical cloud layers, this results in the PP calculation having exactly 32 separate columns (one additional clear-sky column is required). The clear and cloudy fluxes are then averaged according to the cloud fraction overlap following $F^{\uparrow\downarrow} = \Sigma w_i F_i^{\uparrow\downarrow}$, where the index i indicates the overlap weights and $F^{\uparrow\downarrow}$ the upwelling/downwelling fluxes for each column. Note that this calculation method is not identical to the one a GCM would perform, since the GCM averages the fluxes entering clear and cloudy regions at each vertical model layer interface, retaining just two fluxes for the cloudy and clear-sky columns. This involves an implicit and artificial horizontal radiative flux at each layer, rendering the GCM calculation less accurate than the PP calculation performed here. We maintain that the PP method employed in this paper permits a more accurate assessment of the PP bias, since the differences between the IPA and PP methods can only result from the neglect of horizontal inhomogeneity and not from inadequacies in the method of calculation itself. Moreover, recently this method has been implemented operationally in a GCM by *Collins* [2001]. In Figure 2 the CRM field reduced to the "PP mode" is shown. The horizontal axis represents the cloud cover (weight) associated with the column. Although, this calculation uses the assumption of maximum-random overlap in practice only maximum overlap is applied since cloud is present in each vertical layer. Note that the application of maximum overlap produces a smaller total cloud cover of 15% than the true CRM value since the CRM population consists of clouds in all stages of development. This disparity would have been much larger if the simulation had imposed a mean vertical wind shear. *Hogan and Illingworth* [2000] have recently suggested a de-correlation height scale over which cloud reverts to random overlap even if present in adjacent layers. Note how the clear-sky column has an overall weight of around 0.85 showing the low cloud cover of the convection scene.

3. Basic Results: Three-Dimensional Radiative Calculation

3.1. Full Field Analysis

[24] Before analyzing general statistics of the radiative calculations, it is useful to examine details of the radiative fields, to gain an appreciation of the mechanisms involved. To introduce the nature of the 3-D calculation, Figure 3 shows the 2-D radiative vectors for both horizontal and vertical 2-D transects through the domain for the SZA60 case. The two components of these vectors are calculated by integrating the radiance over hemispheres normal to each respective axis. The solar azimuth angle is zero and the Sun is located to the left side of the figure. The vertical slice is for y = 26.2 km and passes through the center of a deep convective event, while the horizontal transect is taken at a height of 2.4 km, in order to appreciate the horizontal extent of the cirrus cloud influence. The shaded contours show the cloud water field (left panels) and heating rates (right panels) to understand how the fluxes are related to the presence of cloud and the energy absorption. Examining the vertical transect, the deep convective events, which extend vertically almost throughout the troposphere, produce a shadowing effect at the surface of about 20 km; consistent with the solar declination angle of 60 degrees, and comparable to the typical resolution of a mesoscale model. In these clear-sky regions, the effect on the heating is marked, which is reduced to almost zero near the cloud because of the opacity of the convective events. The convective clouds exhibit increased heating rates

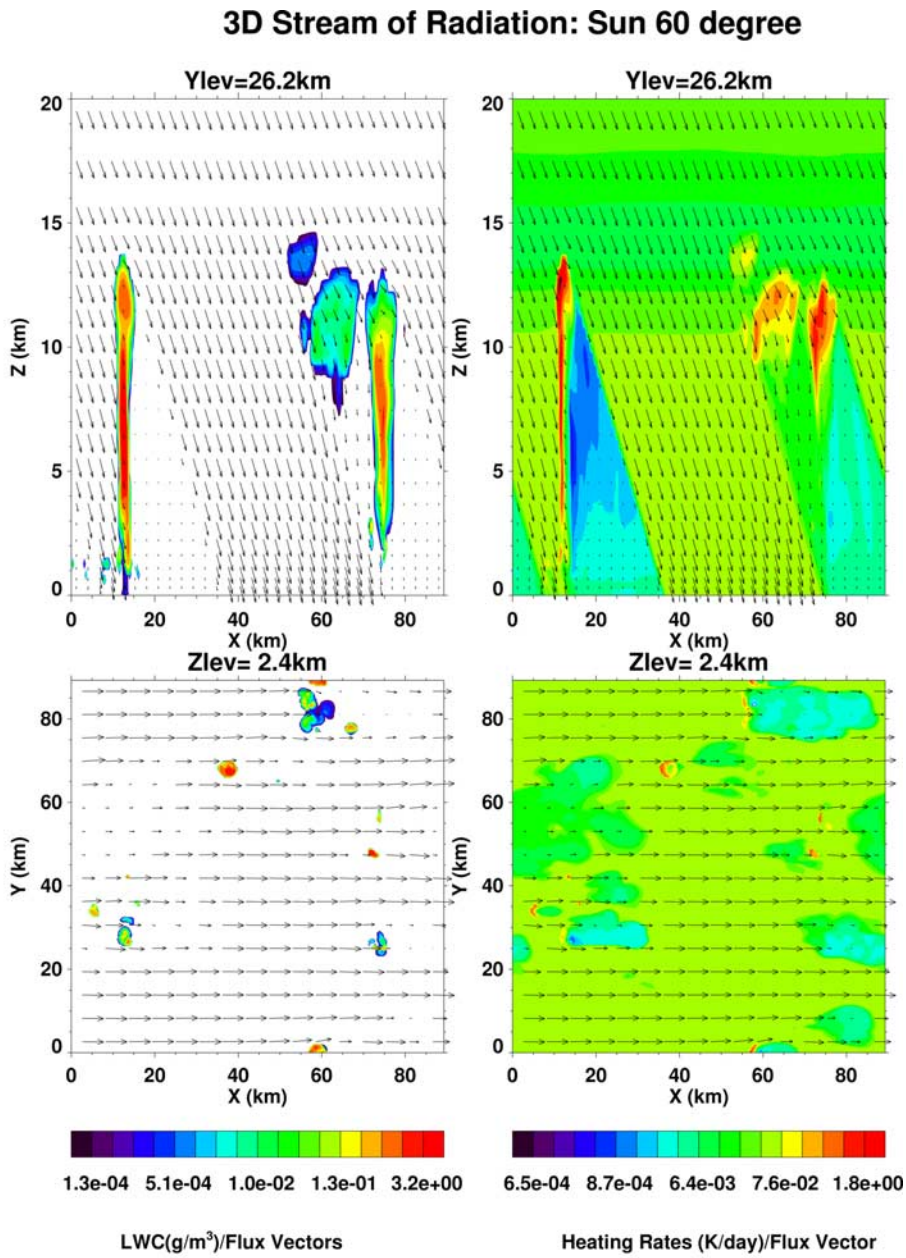

Figure 3. Radiative vectors for both horizontal (upper panel) and vertical (lower panel) sections. Shaded areas represent the transects for the liquid water content (left) and the heating rates (right). The Sun azimuth angle is equal to zero, and the Sun is located to the left side of the figure with SZA60.

throughout their vertical extent, on the other hand, because of the side illumination.

[25] The cirrus anvil remnants situated at $x = 65$ km are less optically opaque and direct radiative transmittance occurs. A change in the direction of the radiative vectors to the vertical is notable, where the horizontal extent of the cirrus is sufficient to extinguish the flux component in this direction. This change in flux direction hints at the presence of regions of flux convergence in the clear-sky regions on the sunny side of the cumulus, which would tend to offset the effect of the cloud shading. The relative magnitude of these effects will obviously depend on the organization of the clouds inside the domain. The horizontal divergence of the fluxes at the top of the two cumulus is also notable, but tends to be a local effect, since this flux is swamped by the larger direct flux in the adjacent clear-sky regions.

[26] The extent of these effects can be appreciated in the horizontal transects. Despite the relatively small cloud cover, the radiative effects are notable over much larger

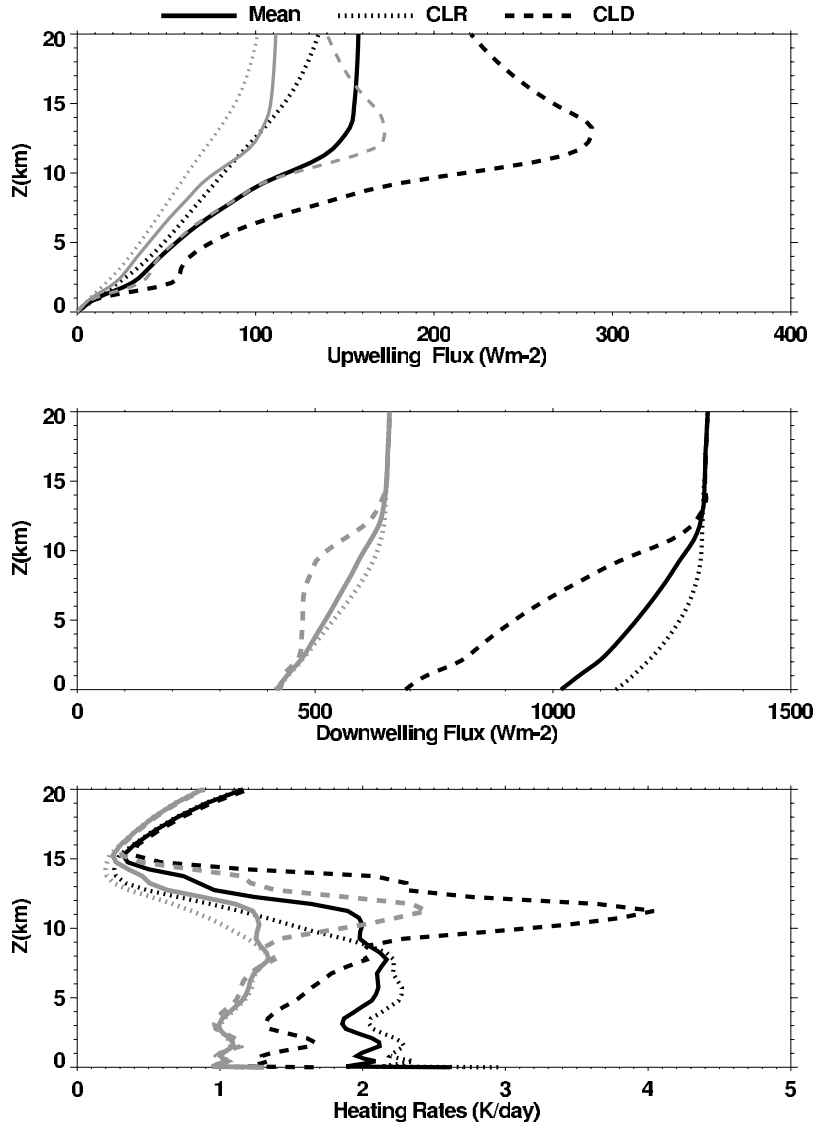

Figure 4. Mean 3-D radiative fluxes and heating rates for the two experiments SZA0 (dark lines) and SZA60 (light lines) across the entire domain and divided into cloudy and clear columns.

regions of the domain, with decreases of clear-sky heating rates exceeding 1 K d^{-1} for significant areas.

3.2. Mean Profiles

[27] To quantify the general observations made in the previous sections, domain and regional mean diagnostics are analyzed. Figure 4 shows mean 3-D radiative fluxes and heating rates for the two experiments: Sun overhead and 60 degrees, averaged across the entire domain and divided into cloudy and clear-sky columns. A cloudy column is defined as any column containing a cloudy point, which is identified using a mass mixing ratio threshold of 10^{-4} kg kg^{-1} for the liquid and ice sum.

[28] The side illumination noted in the transects increases the in-cloud warming in the midtroposphere between 2 and 6 km altitude, relative to the mean heating rate profiles, when compared to the Sun-overhead case. For the lower Sun angle, the clear-sky and cloudy region heating rates are almost identical. This region below the cirrus anvil outflow is shaded in both the Sun-overhead condition and also in 1-D calculations. On the other hand, when the cloud optical thickness is large enough (e.g., the anvils because of their extensive dimensions, and the lower clouds for their large amount of liquid cloud water) then a saturated regime exists. Scattering is then a localized subcloud-scale process and all the available energy is converted into heating. In these situations the local fluxes scale approximately with the cosine of the SZA.

4. One-Dimensional Comparisons

[29] In this section the limitations implicit in commonly used 1-D radiative approximations are assessed. The analysis first addresses local diagnostics, examining horizontal photon transport and 1-D biases along 2-D transects through the cloud field. The 1-D biases are likely to be dependent on the cloud system geometry and an attempt is made to quantify this by calculating radiative statistics as a function of horizontal scale. The emphasis is thus placed on the geometrical effects rather than in-cloud optical inhomogeneities. The

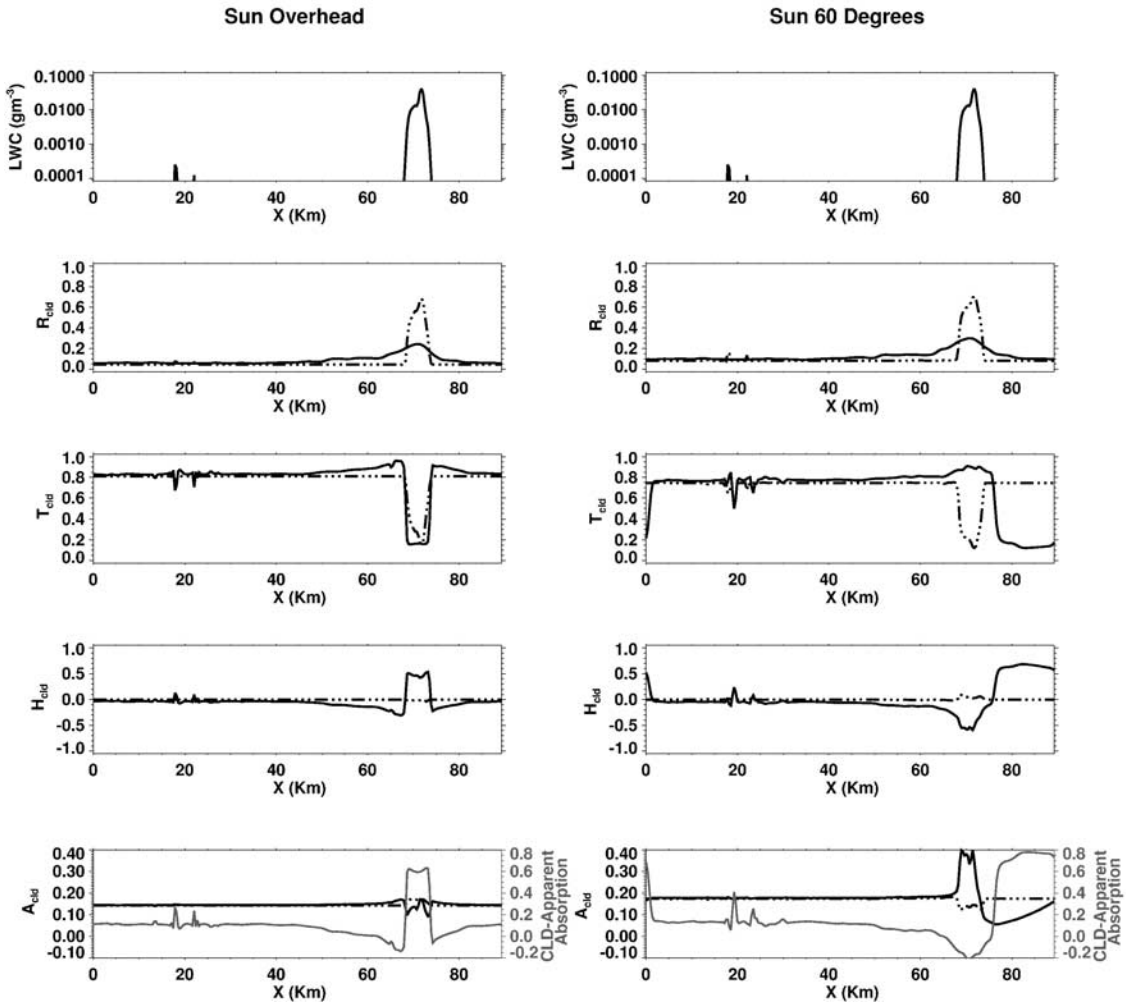

Figure 5. Transect of radiative properties at the cloud boundaries for (left) the SZA0 experiment and (right) the SZA60 experiment. Dotted lines are used for the independent pixel calculations, and solid lines are used for the 3-D ones. Mean LWC (panel 1), reflectance (R_{cld}) (panel 2), transmittance (T_{cld}) (panel 3), and horizontal transport function (H_{cld}) (panel 4) across the transect averaged between the cloud boundaries. Panel 5 shows the cloud absorptance (A_{cld}) and also the apparent absorptance (gray line), as would be evaluated from the differences of flux measurements (see text for details).

lessons learnt from these local diagnostics are then applied to the analysis of traditional domain mean diagnostics.

4.1. Local Diagnostics

4.1.1. Transects

[30] In order to be comparable to GCM radiation codes, measurements of reflectance, transmittance and absorptance have to be averaged over a GCM grid box size. In the cloud scene studied here, the estimation of these three quantities would be strictly dependent on the position of the detectors above and below the cloud and would be greatly influenced by the horizontal fluxes. For example, in Figure 5, statistics for a transect (at $Y = 7$ km) for both experiments are shown between two levels z_1 and z_2 corresponding to cloud top and cloud base, respectively.

[31] For reference, the mean LWC for the transect and the IPA estimations of the same quantities are also reported. The reflectance (R_{z_1}) and transmittance ($T^{z_1}_{z_2}$) are evaluated at these boundaries, while the absorptance ($A^{z_1}_{z_2}$) and horizontal fluxes (normalized by the downward flux) ($H^{z_1}_{z_2}$) are averaged over this layer. These quantities are defined as follows:

$$R_{z_1} = \frac{F^{\uparrow}_{z_1}}{F^{\downarrow}_{z_1}}, \tag{3}$$

$$T^{z_1}_{z_2} = \frac{F^{\downarrow\uparrow}_{z_2}}{F^{\downarrow\uparrow}_{z_1}}, \tag{4}$$

$$H^{z_1}_{z_2} = \frac{1}{\Delta z F^{\downarrow}_{z_1}} \int_{z_2}^{z_1} \nabla F^{\rightleftharpoons}(z)dz, \tag{5}$$

$$A^{z_1}_{z_2} = \frac{1}{\Delta z F^{\downarrow}_{z_1}} \int_{z_2}^{z_1} -\nabla F^{\downarrow\uparrow}(z)dz. \tag{6}$$

$F^{\rightleftharpoons}$ represents the net horizontal flux along the X direction and $F^{\downarrow\uparrow}$ is the net vertical flux. In Figure 6 a schematic of

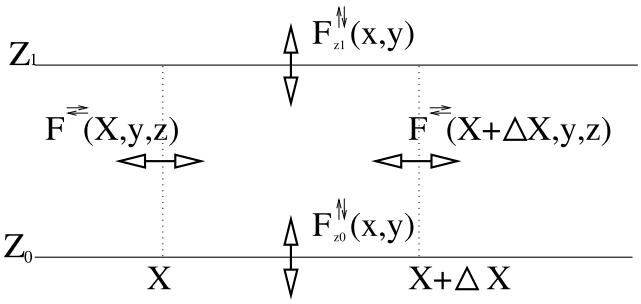

Figure 6. Radiative fluxes at the pixel top, base, and sides through the *x*-*z* planes. The double arrows indicate the net fluxes.

the radiative fluxes at the pixel top, base and sides through the *x*-*z* planes is shown. In equation (6) the cloud absorptance, referring to a subdomain of the full domain, has been derived by integration of the net flux divergence that thus, in the full 3-D calculation, accounts for the horizontal transport of radiation. This quantity is substantially different from the entity termed the ''apparent absorptance'' by *Marshak et al.* [1998], which refers to the column absorptance obtained from a columnar flux difference, as usually derived in measurements. For comparison, Figure 5 also reports the ''apparent absorptance,'' which is higher than the true absorptance in cloudy regions because of flux divergence and significantly lower in clear-sky regions for the opposite reasons, and locally can even be negative.

[32] It is clear that the 1-1 correspondence between the LWC and IPA reflectance/transmittance/absorptance is lost when a 3-D radiative calculation is performed. The reflectance function is smoothed by horizontal transport for both Sun angles and is only very weakly dependent on the cloud geometry. This weak geometrical dependence for the reflectance is a consequence of the fact that the total radiation reflected is a strong function of the upper cloud boundary optical opacity and not of the cloud as a whole, minimizing the effects of cloud shading and cloud-cloud interaction.

[33] Transmittance and absorptance, on the other hand, are strongly dependent on the cloud geometry. When the Sun is overhead, the maximum of the transmittance/absorptance occurs at the cloud boundaries because of the spilling of radiation from the cloud top in the clear areas. In a low-Sun scenario, the transmittance/absorptance are minimized along the shaded projection of the cloud. As already stressed by *Titov* [1998], the horizontal transport is a strong function of neighboring pixel τ and it reaches its maximum (50% of the total incoming energy) on the illuminated side of opaque pixels bordering strong horizontal gradients.

4.1.2. IPA Bias in Two-Dimensional Heating Rates

[34] In broken cloud fields with low cloud cover, diffuse radiation can travel far from the original scattering point. This generates a substantial change in the spatial energy distribution within the domain leading to the creation of areas of flux convergence and/or divergence. To document the heating distribution changes due to horizontal photon transport, snapshots of two-dimensional heating rate differences (3-D − IPA) are reported in Figure 7. The data for the vertical slice is averaged across the Y direction, while the horizontal transects are averaged in the vertical. From the analysis at the two different Sun angles, two different radiative regimes are identified. As seen in the earlier transects, when the Sun is overhead, the spilling of radiation from the cloud anvil creates areas of flux convergence in the adjacent clear regions. The resulting flux divergence in the cloudy regions renders heating rate decreases of up to 1 K d^{-1}. These effects cannot be realized if horizontal transport is neglected. The area of anomalous convergence extends far wider than the cloud boundaries would imply and in fact most of the clear-sky region is influenced. Once deviated from the vertical, the photons can travel unimpeded in the clear columns where no major scattering agents (water droplets or ice) are present. The implication is that the existence of towering clouds can effect areas well-far away from the convection events themselves.

[35] The situation when the Sun is low is more complex. In the 3-D calculation, the vertically extended cloud corresponding to the active convective updrafts below the cirrus anvil are illuminated, and thus experience a large heating increase up to 1 K d^{-1}. This is partially compensated by the extended area of shadow on the far side of the light source. This shadowing regions can extend for tens of kilometers depending on the relative position of the convective events and their aspect ratio, and completely off-set the warming produced by the vertical cross sectional area increase. Figure 8 summarizes schematically the different geometrical regimes in these two cases. It is possible that dynamical consequences could arise from this energy redistribution involving, for example, the mass flux convergence into and out of the cloudy regions [*Gray and Jacobson*, 1977], which has been discussed further by *Tompkins and Di Giuseppe* [2003].

4.1.3. Scale-Dependent Statistics

[36] Current regional or global numerical weather prediction models use grid boxes in the range $O(10)$ km while climate models generally use grids $O(100)$ km. The CRM field therefore has a domain size (89.6 km long) comparable to a GCM grid box.

[37] The significance of the horizontal flux is estimated by calculating the root mean square horizontal flux, normalized by the TOA incoming flux, for increasingly smaller subdomains of horizontal length (ΔL, ΔM):

$$\mathrm{RMS}[H(\Delta L,\Delta M)] = \sqrt{\frac{\Delta L \Delta M}{LM}\sum_{l=1}^{\frac{L}{\Delta L}}\sum_{m=1}^{\frac{M}{\Delta M}}\left(\int_{(l-1)\Delta L}^{l\Delta L}\int_{(m-1)\Delta M}^{m\Delta M} H_{BOA}^{TOA}\,dxdy\right)^2} \tag{7}$$

This indicates how the 3-D bias increases as GCM resolution improves, and is performed for a range of subdomains of decreasing dimension (Figure 9). The error bars reflect the 3% accuracy assessment for the calculation. For the whole CRM domain the residual of the net fluxes at the TOA and BOA and the total column absorptance are equal because of the cyclic boundary conditions. In reality there would be a nonzero horizontal flux divergence, but the magnitude would be limited since the CRM domain exceeds the organization scale of the system analyzed, i.e., the mean separation distance between convective events in this ''unorganized'' deep convective scenario.

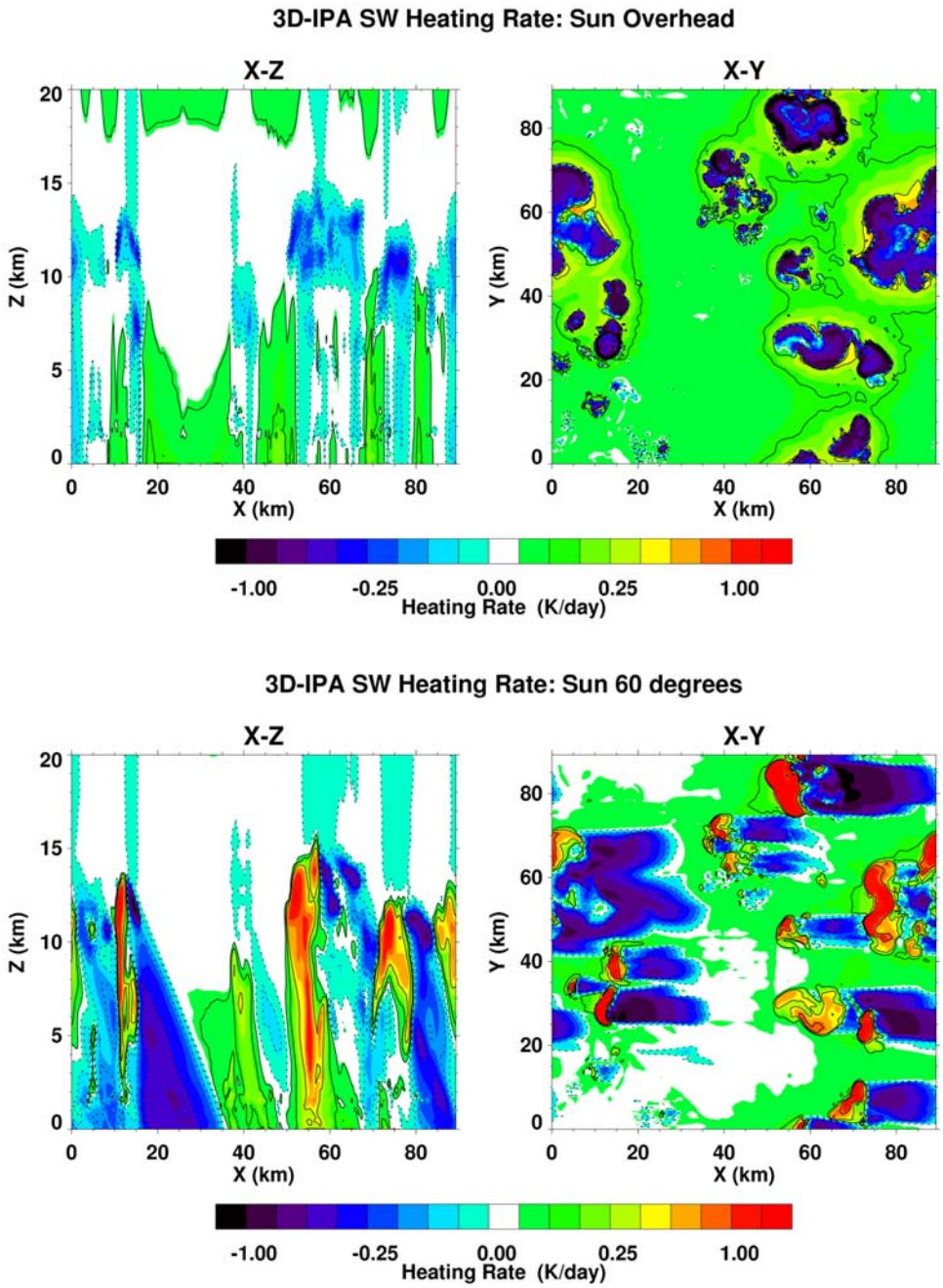

Figure 7. Snapshots of two-dimensional heating rate differences (3-D − IPA) for both solar zenith angles. The data for the *X*-*Z* transect have been averaged along the *Y* direction, while the ones for the *X*-*Y* transect have been averaged along the vertical direction.

[38] For the SZA60 experiment, for example, the importance of the horizontal fluxes increases as the domain length scale decreases with a ratio of 0.15 of the overall incoming fluxes at 25 km domain length, saturating at 0.28 for scales smaller than 5 km. Naturally, these figures would be larger still for a lower Sun zenith angle. Thus for deep convective systems it appears that the horizontal fluxes are nonnegligible as the global and regional model grid resolutions approach the mesoscale.

[39] The direct relationship between the pixel τ and the radiative quantities is essentially lost if 20% of the radiation does not interact locally but instead is transported laterally. *Titov* [1998] found that this effect can create completely erroneous interpretation of experimental data. Analyzing stratocumulus clouds, *Titov* [1998] claimed that a correct assessment of the cloud absorptance can only be obtained by averaging measurements over spatial scales exceeding 6 km over which the horizontal contribution becomes negligible. Examining Figure 9, at 10 km spatial extent the mean contribution of the horizontal flux is still 20% for SZA60 and 10% for SZA0, only becoming negligible when the spatial scale approaches the domain

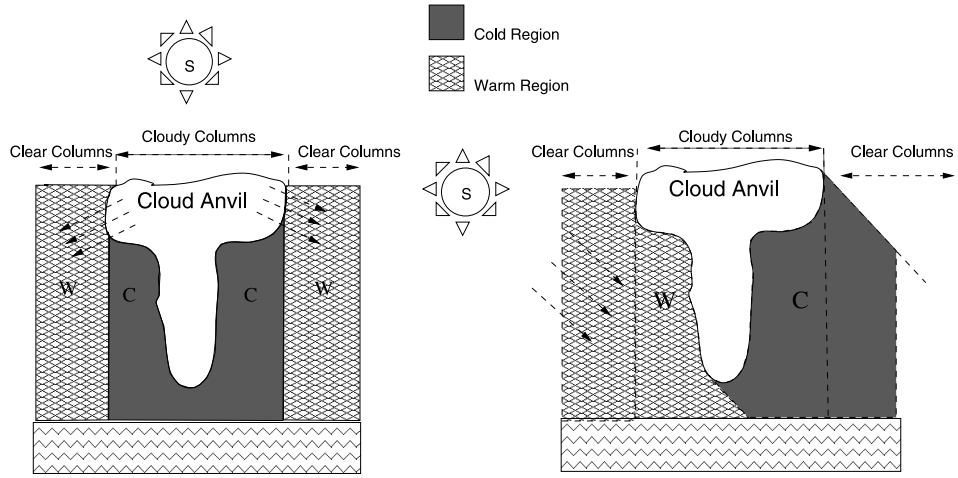

Figure 8. Schematic of the redistribution of the radiation in between clear and cloudy columns: The clear regions surrounding cloudy columns undergo an enhancement of fluxes with an associated warming in the Sun-overhead case due to the "spilling" of radiation from the cloud to the clear region and due to the horizontal transport of photons. The opposite happens when the Sun is set at 60 degree zenith angle, with an increased role of shading, while clear-sky heating rates on the sunny side of the cloud are enhanced.

size, when it is anyway constrained by the periodic boundary conditions.

[40] Note that in the study by *Titov* [1998], the stratocumulus cloud was generated with a fractal bounded cascade model and constituted a single layer 300 m deep, with unity cloud cover. The greater aspect ratio of the deep convective systems examined here will obviously maximize the effect of the horizontal transport, as will the smaller cloud cover. Moreover, the scattered disposition of clouds lacks the periodicity that epitomizes stratocumulus. Cold pool (thermo)dynamics, gravity wave interaction, and feedbacks with water vapor and radiation are just a handful of the many processes that determine the organization of deep convection on a hierarchy of scales. Convection is organized into clusters, and often the clusters into squall lines or mesoscale convective systems with variability expressed over a wide range of scales. With no obvious scale break, averaging over much larger spatial scales, probably approaching $O(100)$ km, would be necessary before horizontal transport could be ignored.

[41] To quantify this scale-dependent bias in terms of heating rates, Figure 10 plots the RMS heating rate error as a function of the subdomain length scale, Δ_L for both Sun angle cases. For both Sun angles the greatest RMS errors occur in the cirrus anvil layer, as one might expect considering cloud cover peaks there, and in the boundary layer, where there is a small secondary peak in cloud cover due to shallow convection and also where the greatest region is affected by anvil shadowing. For the Sun-overhead case there is a obvious transition in the error profiles at around

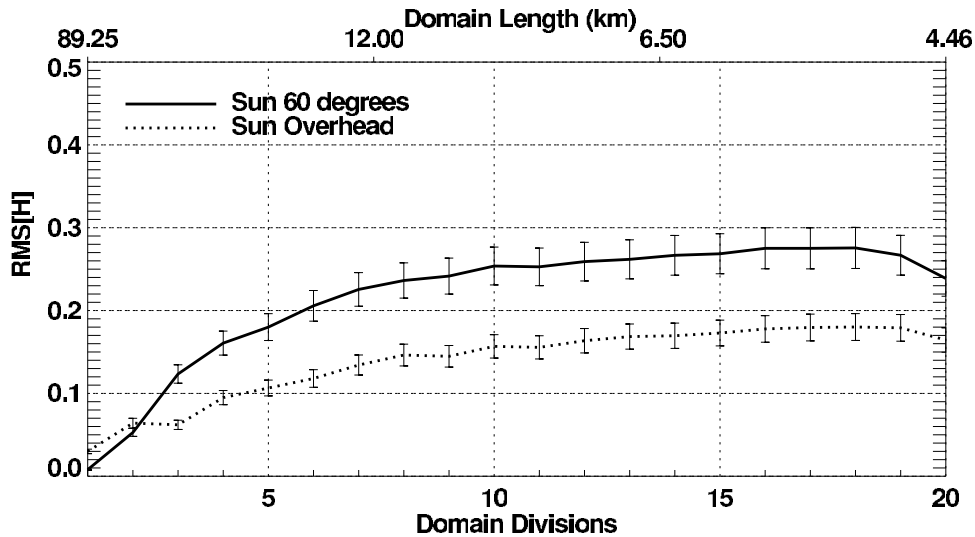

Figure 9. Estimation of the ratio of the horizontal flux to the TOA flux (H) as a function of the subdomain size dimensions.

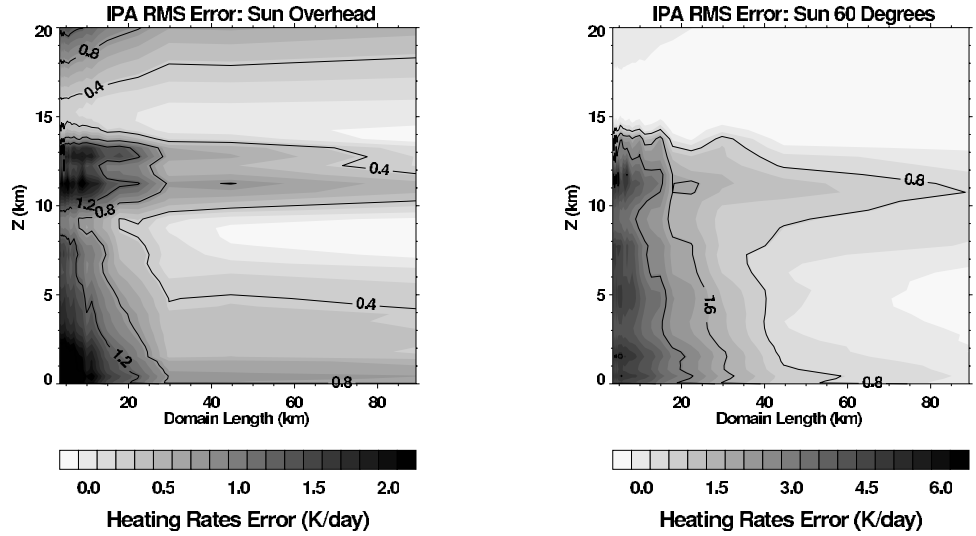

Figure 10. Root mean square heating rate bias as a function of the subdomain length scale for both Sun cases.

$\Delta_L = 20-30$ km. This corresponds to the mode cirrus anvil size of the well developed convective events. For scales greater than this the residual RMS error of up to 0.5 K d^{-1} is principally due to the scattered photon transport. At smaller scales, direct shading by the cirrus dominates and RMS errors approach 2 K d^{-1}. There is a clear double-peaked signal in the cirrus region clearly demarking the anvil cloud upper and lower boundaries. With the lower Sun angle the general distribution of the RMS error is similar to the Sun-overhead case, but there is no clear demarkation of the cirrus anvil dimension. Relative to the Sun-overhead case, RMS IPA heating rate errors at this low Sun angle are almost three times larger when small horizontal spatial scales are considered, peaking at 6 K d^{-1}. Note how the stratospheric errors are actually smaller.

4.2. Domain-Average Diagnostics

4.2.1. Flux and Heating Rate Profiles

[42] The local diagnostics have shown how the horizontal transport can create regions of flux convergence and divergence, as discussed previously by *Vogelmann et al.* [2001]. The ultimate consequence of these opposing effects (shadowing and side illumination) is assessed with domain-averaged statistics. In Figure 11 the 3-D − IPA differences (left column) and the 3-D − IPA root mean square differences (right column) in the mean upwelling/downwelling fluxes and heating rates profiles are reported. The mean profiles have also been calculated for clear and cloudy columns. Despite significant local 3-D effects, domain-averaged differences are smaller. The significant in-cloud IPA bias has a more limited influence on the domain average statistics since it applies only to a small fraction of the domain, and is of opposite sign to the clear-sky signal as expected. The overall relative IPA biases are around 5–10%, compared to peak values exceeding 20% in the lower levels of the cloudy columns in experiment SZA60. Thus, even in domain-averaged quantities, 3-D effects are nonnegligible. The total influence of the horizontal transport can be more easily appreciated by looking at the root mean square of the IPA bias (right column,

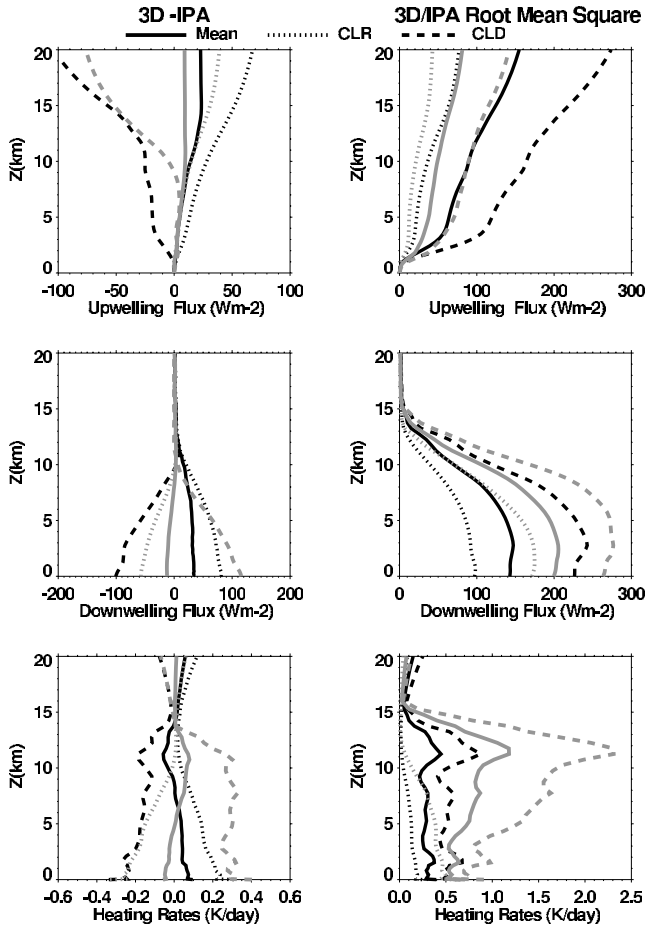

Figure 11. 3-D − IPA differences (left column) and the 3-D − IPA root mean square differences (right column) in the mean upwelling/downwelling fluxes and heating rates profiles. The dark lines are used for the SZA0 experiment, while light lines are used for the SZA60 experiment.

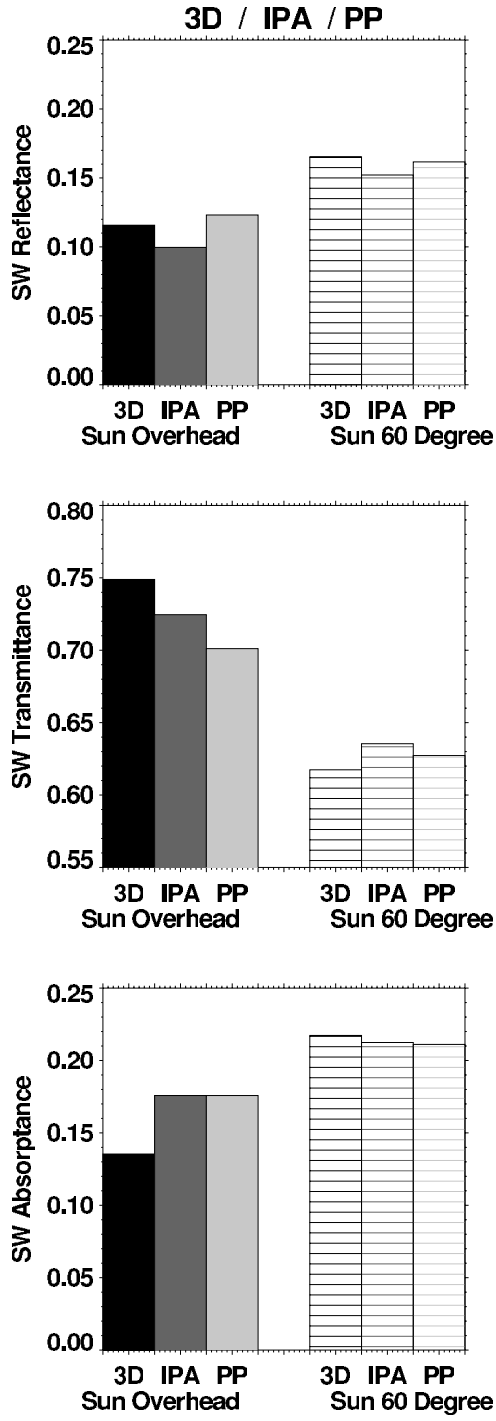

Figure 12. Reflectance, transmittance, and absorptance for the two experiments SZA0 and SZA60. The calculation is performed for the whole domain using the full 3-D radiative transfer, the independent pixel approximation (IPA), and plane-parallel (PP) methods.

Figure 11). In this case the differences can easily attain 50% of the domain average and as much as 100% if the averaging is performed on cloudy columns only (for experiment SZA60). In general, the different sign of the biases reflects the characteristics of Figure 5 with a heating rate increase observed when the Sun position is low, and a decrease occurring when the Sun is overhead. In fact, from the analysis of the local energy redistribution it is clear that the final mean domain quantities depend on several geometrical factors such as the cloud aspect ratio, the inter-cloud distances and the Sun zenith angle.

4.2.2. Atmospheric Reflectance, Transmittance, and Absorptance

[43] The radiative properties of reflectance, transmittance and absorptance are given in Figure 12, while Table 1 gives the magnitude of the biases. The PP bias is simple to interpret from the convex nonlinearity of the reflectance and the concavity of the transmittance as function of τ. Inhomogeneous clouds are always darker than their homogeneous counterpart. Consequently, ΔR_{PP} is always smaller than zero while ΔT_{PP} is constrained to be positive. Differences of 19% are found for the PP bias in the reflectance for SZA0 and of around 6% for SZA60. The PP bias in the reflectance is largely offset by changes in transmittance, with limited changes in absorption. The situation is more complex for the IPA bias. The sign and magnitude of the biases are controlled by the horizontal transport systematic behavior. The reflection of the cloud scene is enhanced in both Sun scenarios when a full 3-D calculation is performed while the change in transmission at the surface is strongly affected by the Sun position. In the solar spectral region and for deep convective systems the IPA assumption leads to an underestimation of the total transmission for high Sun angles and an overestimation for low Sun positions. This behavior was also found in the ultraviolet spectral region by *Scheirer and Macke* [2001]. It is apparent that the IPA bias is of the same order of significance than the PP bias for both reflectance and transmittance, despite the cancellation of errors noted earlier, while it becomes the major source of uncertainty when an assessment on the atmospheric absorption is required.

5. Discussion and Conclusions

[44] In this study we have analyzed the effect of 3-D radiative transfer through a tropical deep convective system generated from a three-dimensional cloud-resolving model. In the few examples in which these cloud fields have been studied previously, the results have been quite contrasting, possibly because of the peculiarities of the cloud scenes examined, characterized in some cases by high cloud cover or the limitations imposed by satellite imagery retrieval. For this reason, the aim of this study was to use a detailed and well-resolved cloud field generated by a high-resolution 3-D CRM to attempt to quantify more rigourously the mechanisms involved, and their relative importance, in the 3-D transport of energy. A case was chosen which is expected to maximize the 3-D effect, with deep convective events characterized by low anvil cloud coverage.

[45] The aspect ratio of towering clouds and their organization in small-scale clusters can create substantial radiative differences when horizontal transport of photons is accounted for. In fact, significant energy redistribution inside the cloudy and clear regions is found when a full 3-D calculation is performed, relative to one-dimensional calculations. This redistribution is also responsible for the loss of correspondence between the cloud water content in a column and its radiative properties.

Table 1. Reflectance, Transmittance, and Absorptance for IPA and PP Biases for Both Experiments SZA0 and SZA60[a]

	IPA Bias SZA0		PP Bias SZA0		IPA Bias SZA60		PP Bias SZA60	
	Abs	Rel, %	Abs	Rel, %	Abs	Rel, %	Abs	Rel, %
Reflectance	0.016	16	−0.023	−19	0.013	8.6	−0.0095	−5.9
Transmittance	0.024	3.4	0.023	3.5	−0.018	−2.8	0.0082	1.3
Absorptance	−0.040	−23	0.0	0.0	0.0049	2.3	0.0013	0.63

[a]Abs, absolute; rel, relative.

[46] Another effect of this local energy variability is the creation of hot spots where significantly enhanced flux convergence takes place, controlled by the combination of the Sun position, the cloud aspect ratio and the inter-cloud distances, as also reported by *Vogelmann et al.* [2001]. At a SZA of 60 degrees, the IPA calculation gives larger heating rates than the associated 3-D calculation in clear regions and smaller in cloudy regions, while with the Sun overhead the opposite is true. These effects point to the increased role that shading takes in cloud systems that have aspect ratios approaching unity.

[47] The relative roles of the shading and convergence regions was not appreciable in previous investigations using model generated cloud fields that were overcast. In contrast to horizontally extended clouds, these tall and optically thick deep convective systems produce extensive shading at low Sun angles, responsible for local heating decreasing of as much as 1 K d^{-1}, which may be partially compensated for by increased flux convergence on the illuminated side of the cloud. On the other hand, when the Sun is overhead the spilling of radiation from the cloud anvil can produce a decrease of heating from the cloud top of as much as 1 K d^{-1} associated with an extended increase of radiation in the clear regions distant from the cloud boundaries.

[48] Analyzing averaged domain quantities we still find that 3-D radiative transfer has a nonnegligible effect, particularly at lower levels, where differences of up to 20% are noted for the cloudy columns and 15% for the clear sky with a SZA equal to 60 degrees, which is equivalent to a heating rate differences of approximately 0.4 K d^{-1}. These differences substantially exceed those previously reported by *Barker et al.* [1999] and *Fu et al.* [2000] for deep convective cases, presumably as a result of the different cloud geometry and lower cloud cover in the situation investigated here. The importance of these biases is clearly related to the scale of cloud organization inside the domain and the balance of the two opposing effects. For this reason the study of one unique cloud scene cannot be considered a conclusive assessment of 3-D radiative effects. By supplementing the previous overcast or cloud-sparse scenes with the field investigated here, which contains a realistic distribution of deep convective events, with typical anvil diameters of 15 to 30 km, a better appreciation of the range of possible IPA biases is gained. In organized deep convective systems, such as mesoscale convective systems, or squall lines, that can produce outflow generated cirrus extending many hundreds of kilometers, the previous smaller assessments of IPA bias made in overcast skies may be applicable. On the other hand, for situations of isolated events which are largely unorganized, which during the Tropical Ocean Global Atmosphere Coupled Ocean-Atmosphere Response Experiment (TOGA COARE) were observed to constitute approximately 50% of all convective events [*Rickenbach and Rutledge*, 1998], the larger IPA biases documented here are more likely to be appropriate.

[49] This study, together with its predecessors, only examine a handful of cloud scenes, using different radiative models and associated assumptions in each case. The magnitude of the radiative biases reported here from a single cloud scene can only be indicative and cannot be taken as definitive. A more systematic documentation of IPA bias would require a full investigation of the parameter space of in-cloud optical variability and organization of the cloud inside the domain. A controlled investigation of parameter space implies the use of an idealized model for cloud generation, since controlling organization factors is highly challenging in observations or complex numerical models. Previous idealized studies were mostly based on simple geometric cloud shapes [e.g., *Kite*, 1987], with many degrees of freedom rendering parameter space investigation unattainable, or fractal cloud models [e.g., *Cahalan et al.*, 1994b; *Marshak et al.*, 1998] with no vertical structure; the cloud consisting of a single, vertically uniform slab. An accompanying paper [*Di Giuseppe and Tompkins*, 2003] thus attempts to introduce a new idealized model which addresses these weaknesses, which is used initially to investigate the influence of stratocumulus organizational scales on radiative transfer biases.

[50] **Acknowledgments.** The radiation calculation was performed at Manchester Supercomputer facilities with the use of UGAMP resources, and Lois Steenman-Clark is thanked for arranging this provision. Frank Evans is thanked for providing his code publicly and his advice concerning its use. The Met Office (UK) supplied the cloud-resolving model used to generate the cloud field. The support of Keith Shine, Anthony Slingo, and Kevin Hodges is appreciated. During this research work the first author was supported by NERC studentship GT/4/00/217.

References

Aida, M. A., Scattering of solar radiation as a function of cloud dimension and orientation, *J. Quant. Spectrosc. Radiat. Transfer*, *17*, 303–310, 1977.

Barker, H. W., J. J. Morcrette, and G. D. Alexander, Broadband solar fluxes and heating rates for atmospheres with 3D broken clouds, *Q. J. R. Meteorol. Soc.*, *124*, 1245–1271, 1998.

Barker, H. W., G. L. Stephens, and Q. Fu, The sensitivity of domain-averaged solar fluxes to assumptions about cloud geometry, *Q. J. R. Meteorol. Soc.*, *125*, 2127–2152, 1999.

Benedetti, A., and G. L. Stephens, Characterization of errors in cirrus simulations from a cloud resolving model for application in ice water content retrievals, *Atmos. Res.*, *59*, 393–417, 2001.

Benedetti, A., G. L. Stephens, and J. M. Haynes, Ice cloud microphysics retrievals from millimeter radar and visible optical depth using an estimation theory approach, *J. Geophys. Res.*, *108*(D11), 4335, doi:10.1029/2002JD002693, 2003.

Brown, P. R. A., and A. J. Heymsfield, The microphysical properties of tropical convective anvil cirrus: A comparison of models and observations, *Q. J. R. Meteorol. Soc.*, *127*, 1535–1550, 2001.

Brown, P. R. A., and H. A. Swann, Evaluation of key microphysical parameters in three dimensional cloud model simulations using aircraft and multiparameter radar data, *Q. J. R. Meteorol. Soc.*, *123*, 2245–2275, 1997.

Brown, R. G., and C. Zhang, Variability of midtropospheric moisture and its effect on cloud-top height distribution during TOGA COARE, *J. Atmos. Sci.*, *54*, 2760–2774, 1997.

Byers, H. R., and R. R. Braham Jr., Thunderstorm structure and circulation, *J. Meteorol.*, *5*, 71–86, 1948.

Cahalan, R. F., W. Ridgway, and W. J. Wiscombe, Independent pixel and Monte Carlo estimate of stratocumulus albedo, *J. Atmos. Sci.*, *51*, 3776–3790, 1994a.

Cahalan, R. F., W. Ridgway, W. J. Wiscombe, T. L. Bell, and J. B. Snider, The albedo of fractal stratocumulus clouds, *J. Atmos. Sci.*, *51*, 2434–2455, 1994b.

Carlin, B., Q. Fu, U. Lohmann, G. G. Mace, K. Sassen, and J. M. Comstock, High-cloud horizontal inhomogeneity and solar albedo bias, *J. Clim.*, *15*, 2321–2339, 2002.

Chambers, L. H., B. A. Wielicki, and K. F. Evans, Accuracy of the independent pixel approximation for satellite estimates of oceanic boundary layer cloud optical depth, *J. Geophys. Res.*, *102*, 1779–1794, 1997.

Coakley, J. A., and R. Davies, The effect of cloud sides on reflected solar radiation as deduced from satellite observations, *J. Atmos. Sci.*, *43*, 1025–1035, 1986.

Collins, D. W., Parameterization of generalized cloud overlap for radiative calculations in general circulation models, *J. Atmos. Sci.*, *58*, 3224–3242, 2001.

Davis, A., A. Marshak, R. Cahalan, and W. Wiscombe, The Landsat scale break in stratocumulus as a three-dimensional radiative transfer effect: Implications for cloud remote sensing, *J. Atmos. Sci.*, *54*, 241–260, 1997.

Di Giuseppe, F., and A. M. Tompkins, Effect of spatial organization on solar radiative transfer in three-dimensional idealized stratocumulus cloud fields, *J. Atmos. Sci.*, *60*, 1774–1794, 2003.

Diongue, A., J.-P. Lafore, J.-L. Redelsperger, and R. Roca, Numerical study of a sahelian synoptic weather system: Initiation and mature stages of convection and its interactions with the large-scale dynamics, *Q. J. R. Meteorol. Soc.*, *128*, 1899–1927, 2002.

Donner, L. J., C. J. Seman, and R. S. Hemler, Three-dimensional cloud-system modeling of GATE convection, *J. Atmos. Sci.*, 56, 1885–1912, 1999.

Emanuel, K. A., *Atmospheric Convection*, 580 pp., Oxford Univ. Press, New York, 1994.

Evans, K. F., The spherical harmonics discrete ordinate method for three-dimensional atmospheric radiative transfer, *J. Atmos. Sci.*, *55*, 429–446, 1998.

Fu, Q., and K. N. Liou, On the correlated k-distribution method for radiative-transfer in nonhomogeneous atmospheres, *J. Atmos. Sci.*, *49*, 2139–2156, 1992.

Fu, Q., M. C. Cribb, H. W. Barker, S. K. Krueger, and A. Grossman, Cloud geometry effects on atmospheric solar absorption, *J. Atmos. Sci.*, *57*, 1156–1168, 2000.

Grabowski, W. W., X. Wu, M. W. Moncrieff, and W. D. Hall, Cloud-resolving modeling of cloud systems during phase III of GATE. Part II: Effects of resolution and the third spatial dimension., *J. Atmos. Sci.*, *55*, 3264–3282, 1998.

Gray, W. M., and W. M. Jacobson Jr., Diurnal-variation of deep cumulus convection, *Mon. Weather Rev.*, *105*, 1171–1188, 1977.

Hogan, R. J., and A. J. Illingworth, Deriving cloud overlap statistics from radar, *Q. J. R. Meteorol. Soc.*, *126*, 2903–2909, 2000.

Houze, R. A., Jr., Structures of atmospheric precipitation systems: A global survey, *Radio Sci.*, *16*, 671–689, 1981.

Johnson, R. H., T. M. Rickenbach, S. A. Rutledge, P. E. Ciesielski, and W. H. Shubert, Trimodal characteristics of tropical convection, *J. Clim.*, *12*, 2397–2418, 1999.

Kite, A., The albedo of broken cloud fields, *Q. J. R. Meteorol. Soc.*, *113*, 517–531, 1987.

Liao, X., and D. Rind, Local upper tropospheric/lower stratospheric clear-sky water vapor and tropospheric deep convection, *J. Geophys. Res.*, *102*, 19,543–19,557, 1997.

Liou, K. N., S. C. Ou, Y. Takano, J. Roskovensky, G. G. Mace, K. Sassen, and M. Poellot, Remote sensing of three-dimensional inhomogeneous cirrus clouds using satellite and mm-wave cloud radar data, *Geophys Res Lett.*, *29*(9), 1360, doi:10.1029/2002GL014846, 2002.

Luo, Y. L., S. K. Krueger, G. G. Mace, and K. M. Xu, Cirrus cloud properties from a cloud-resolving model simulation compared to cloud radar observations, *J. Atmos. Sci.*, *60*, 510–525, 2003.

Mace, G. G., T. P. Ackerman, P. Minnis, and D. F. Young, Cirrus layer microphysical properties derived from surface-based millimeter radar and infrared interferometer, *J. Geophys. Res.*, *103*, 23,207–23,216, 1998.

Marshak, A., A. Davis, W. Wiscombe, W. Ridgway, and R. F. Cahalan, Biases in short-wave column absorption in the presence of fractal clouds, *J. Clim.*, *11*, 431–446, 1998.

McClatchey, R. A., R. W. Fenn, J. E. A. Selby, F. E. Volz, and J. S. Garing, Optical properties of the atmosphere, *Tech. Rep. AFCRL-72-0497*, Hanscom Air Force Base, Bedford, Mass., 1972.

McKee, T. B., and S. K. Cox, Scattering of visible radiation by finite clouds, *J. Atmos. Sci.*, *31*, 1885–1892, 1974.

Montmerle, T., J. P. Lafore, and J. L. Redelsperger, A tropical squall line observed during TOGA COARE: Extended comparisons between simulations and Doppler radar data and the role of midlevel wind shear, *Mon. Weather Rev.*, *128*, 3709–3730, 2000.

O'Hirok, W., and C. Gautier, A three-dimensional radiative transfer model to investigate the solar radiation within a cloudy atmosphere. Part I: Spatial effects, *J. Atmos. Sci.*, *55*, 2162–2179, 1998a.

O'Hirok, W., and C. Gautier, A three-dimensional radiative transfer model to investigate the solar radiation within a cloudy atmosphere. Part II: Spectral effects, *J. Atmos. Sci.*, *55*, 3065–3076, 1998b.

Ovtchinnikov, M., and Y. L. Kogan, Evaluation of radar retrieval algorithms in stratiform clouds using large-eddy simulations, *J. Geophys. Res.*, *105*, 17,351–17,359, 2000.

Phillips, V. T. J., A. M. Blyth, P. R. A. Brown, T. W. Choularton, and J. Latham, The glaciation of a cumulus cloud over New Mexico, *Q. J. R. Meteorol. Soc.*, *127*, 1513–1534, 2001.

Redelsperger, J. L., et al., A GCSS model intercomparison for a tropical squall line obsrved during TOGA-COARE. I: Cloud-resolving models, *Q. J. R. Meteorol. Soc.*, *126*, 823–863, 2000.

Rickenbach, T. M., and S. A. Rutledge, Convection in TOGA-COARE: Horizontal scale, morphology, and rainfall production, *J. Atmos. Sci.*, *55*, 2715–2729, 1998.

Sassen, K., Z. Wang, V. I. Khvorostyanov, G. L. Stephens, and A. Bennedetti, Cirrus cloud ice water content radar algorithm evaluation using an explicit cloud microphysical model, *J. Appl. Meteorol.*, *41*, 620–628, 2002.

Scheirer, R., and A. Macke, On the accuracy of the independent column approximation in calculating the downward fluxes in the UVA, UVB and PAR spectral ranges, *J. Geophy. Res.*, *106*, 14,301–14,312, 2001.

Shutts, G. J., and M. E. B. Gray, A numerical modelling study of the geostrophic adjustment following deep convection, *Q. J. R. Meteorol. Soc.*, *120*, 1145–1178, 1994.

Stubenrauch, C. J., A. D. Delgenio, and W. B. Rossow, Implementation of subgrid cloud vertical structure inside a GCM and its effect on the radiation budget, *J. Clim.*, *10*, 273–287, 1997.

Swann, H., Sensitivity to the representation of precipitating ice in CRM simulations of deep convection, *Atmos. Res.*, *48*, 415–435, 1998.

Titov, G., Radiative horizontal transport and absorption in stratocumulus clouds, *J. Atmos. Sci.*, *55*, 2549–2560, 1998.

Tompkins, A. M., The impact of dimensionality on long-term cloud resolving model simulations, *Mon. Weather Rev.*, *128*, 1521–1535, 2000.

Tompkins, A. M., Organization of tropical convection in low vertical wind shears: The role of coldpools, *J. Atmos. Sci.*, *58*, 1650–1672, 2001.

Tompkins, A. M., and G. C. Craig, Radiative-convective equilibrium in a three-dimensional cloud ensemble model, *Q. J. R. Meteorol. Soc.*, *124*, 2073–2097, 1998.

Tompkins, A. M., and F. Di Giuseppe, Solar radiative biases in deep convective regimes: Possible implications for dynamical feedback, *Q. J. R. Meteorol. Soc.*, *129*, 1721–1730, 2003.

Vogelmann, A. M., V. Ramanathan, and I. A. Podgorny, Scale dependence of solar heating rates in convective cloud systems with implications to general circulation models, *J. Clim.*, *14*, 1738–1752, 2001.

Wang, Z., and K. Sassen, Cirrus cloud microphysical property retrieval using lidar and radar measurements. Part I: Algorithm description and comparison with in situ data, *J. Appl. Meteorol.*, *41*, 218–229, 2002.

Welch, R. M., and B. A. Wielicki, A radiative parameterization of stratocumulus cloud field, *J. Atmos. Sci.*, *42*, 2888–2897, 1985.

Welch, R. M., and B. A. Wielicki, Reflected fluxes for broken clouds over a Lambertian surface, *J. Atmos. Sci.*, *46*, 1384–1395, 1989.

Zhang, C. D., Large-scale variability of atmospheric deep convection in relation to sea surface temperature in the tropics, *J. Clim.*, *6*, 1898–1913, 1993.

Zuidema, P., and K. F. Evans, On the validity of the independent pixel approximation for boundary layer clouds observed during ASTEX, *J. Geophys. Res.*, *103*, 6059–6074, 1998.

F. Di Giuseppe, Environmental Systems Science Centre, University of Reading, Reading RG6 6AL, UK. (fdg@mail.nerc-essc.ac.uk)

A. M. Tompkins, European Centre for Medium-Range Weather Forecasts, Shinfield Park, Reading RG2 9AX, UK. (adrian.tompkins@ecmwf.int)